

Stability analysis under thermogravitational effect

B. Šeta¹, Jna. Gavalda¹, M.M.Bou-Ali², X. Ruiz¹

¹ Universitat Rovira i Virgili, Tarragona, Spain

² Mondragon Unibersitatea, Mondragon, Spain

berin.seta@urv.cat

mbouali@mondragon.edu

Abstract

In the present work, an interferometric unsteady analysis of the thermogravitational technique was for the first time attempted in a paralelepipedic microcolumn using binary mixtures with negative Soret coefficients. In particular, water/ethanol and toluene/methanol were considered, as they have significantly different thermophysical properties and relaxation times. Experiments were run with different temperature gradients in order to understand their impact on the stability of separation. Experimental results were compared with theoretical ones, predicted by Fury-Jones-Onsager theory, and by OpenFOAM 3D numerical simulations. Correlations between the separation and the flow in the third dimension perpendicular to the thermal gradient of the thermogravitational microcolumn were analysed. Numerical simulations were also conducted in traditional cylindrical columns in order to compare the results with those previously reported. In these cases, the impact on separation stability was correlated with the azimuthal component of velocity. Thus, in both configurations, the disturbing convective current, always generated in the direction perpendicular to the thermal gradient applied, was shown to be vital for flow stability analysis.

1. Introduction

It is well known that the Soret effect induces changes in the concentration field under the influence of temperature gradients. Some molecules are attracted to the cold wall, while others goes toward hot wall. In the mixtures this effect can lead to separation of individual components. Soret effect was found in 1879 [1] using a simple experiment with a water/salt solution. But, it is also present in a number of different natural phenomena, including ocean movements, convection in stars, solar ponds and hydrocarbon reservoirs [2-5]. The Soret effect is also used in biological flows as, for instance, a separation factor in microfluidic devices and to remove cryoprotectants from biological fluids [6].

From a mathematical point of view the mass flux of a binary mixture subjected to a temperature gradient can be written as:

$$J = -\rho D \nabla c - \rho D_T c_0 (1 - c_0) \nabla T \quad (1)$$

In the steady state, $J=0$, so equation (1) can be rewritten in the form:

$$\nabla c = -\frac{D_T}{D} c_0 (1 - c_0) \nabla T \quad (2)$$

Where c is the concentration of the denser component, c_0 represents the mean concentration of the component with a higher density. The ratio between thermodiffusion D_T and molecular diffusion D coefficients is defined as Soret coefficient $S_T = \frac{D_T}{D}$. As changes in concentration field are small enough, change of coefficients can be assumed as linear. In that case, we take diffusion and thermodiffusion coefficients as constant mean value. There are a few different techniques available in the literature that could measure such transport properties, mainly divided into two categories: convectionless methods and methods by which convection promotes separation [7]. Convectionless techniques include Optical Digital Interferometry (ODI) [8], the Optical Beam Deflection Technique (OBD) [9] and the Thermal Diffusion Forced Rayleigh Scattering Technique (TDFRS) [10]. Alternatively, the Rayleigh-Bernard [11, 12] setup and thermogravitational columns (TGC) [13, 14] are convection-based techniques, the latter of which was used in this work.

There are two possible behaviours for the mixture inside a thermogravitational column, depending on the sign of the Soret coefficient. In this work, we focused on negative Soret coefficients [15]. When a binary mixture exhibits this particular behaviour, the heavier component will migrate towards the hot wall and, due to advection, will be enriched in the top part of the column. **In the binary mixture, such behaviour will lead to an adverse density stratification.** The main aim of this work was thus to experimentally and numerically observe whether this arrangement can lead to a stable steady state in which Furry-Jones-Onsager (FJO) theory can be used to determine thermodiffusion coefficients.

Few studies in the literature have addressed this problem. Experimentally, only TGC studies performed by Bou-Ali [16, 17] on benzene/ethanol, benzene/methanol, toluene/ethanol, toluene/methanol and water/ethanol mixtures in a broad range of concentrations are available. One report [17] determined a negative range of values for those mixtures, which corresponds fairly well with other results in the literature for the same mixtures. Apart from these experimental studies, a few theoretical studies have been conducted as well regarding stability analysis in thermogravitational columns. One of the first was conducted by Rudakov [18, 19] regarding pure liquids. Convective stability analyses of a binary incompressible fluid on normal perturbations to a thermal gradient were performed later by Nikolaev and Tubin [20] and accounted for the dependency on a concentration gradient. Gershuni et al. [21] examined a binary mixture in which the buoyancy force was a function of temperature difference only. More recently, a similar type of analysis, which included two- and three-dimensional perturbations to steady state solutions, was performed by Batiste et al. [22]. They concluded that a thermogravitational steady state with negative Soret coefficients was always unstable when the steady state was set against 3D perturbations. Zebib stability analysis for binary mixtures [23] with 2D disturbances was extended in [24] on multicomponent mixtures and 3D disturbances. In that work, correlations for the onset of longitudinal and transverse instabilities were reported. Ryzkhov et al. analysed binary and multicomponent instabilities with long-wave perturbations [25], which was extended to 3D perturbations in [26] for a broad range of input parameters. Finally, Zebib et al. [27] checked the stability of convection with negative Soret numbers with enhanced separation in inclined thermogravitational columns. Theoretical study regarding steady-state measurement in thermogravitational column [28] and transient analysis with forgotten effect included [29] is made by Haugen et al.. Theoretical work on multicomponent separation in traditional cylindrical columns [30] and transient analysis [31] have been conducted by Kozlova et al..

In the present work, the complete process of transient separation was experimentally attempted for the first time inside a transparent paralelepipedic microcolumn for mixtures with negative Soret coefficients. The results were compared with fully 3D numerical simulations conducted in OpenFOAM. Special focus was placed on the existence of stable separation in both experimental and numerical studies. Disturbance of the velocity field, especially in the third dimension perpendicular to the thermal gradient, was considered. Also, the concentration and velocity profiles in the planes perpendicular to a temperature gradient were compared for different breadths of the column. Conclusions were made out about the role of the breadth column in the stabilisation of the flow.

In addition to flow analysis in the paralelepipedic microcolumn, a numerical study in cylindrical thermogravitational columns [16, 17] was compared with our experimental results. A similar systematics as described before was used here, one in which flow differences were examined for different ratios between the radius of both inner and outer cylinders.

Results are compared with Furry-Jones-Onsanger theory which is used to determine thermodiffusion coefficients from steady-state measurements. Theory explained that after certain time convection in the column will reach steady-state making it possible to determine vertical difference in concentration for binary mixtures. By applying

$$D_T = \frac{\beta_T g d^4}{504 v c_0 (1 - c_0)} \cdot \frac{\partial c}{\partial z} \quad (3)$$

where d is gap, β_T is thermal expansion coefficient and v is the kinematic viscosity. Originally, theory assumed that density is only in the function of temperature and not in function of the concentration. This situation refers in thermodiffusion community as “forgotten effect”. Since FJO theory neglected composition effect in buoyancy term, both possible situations regarding sign of Soret coefficient were “stable”. However, in reality for binary mixture when Soret coefficient is negative, more dense component migrates to the hot wall and advect on the top of the column creating adverse gradient of density.

The work will be consisted from two main parts; first part is related with experimental and numerical analysis of separation stability in microcolumn. In this part, two different mixtures are considered, toluene/methanol (2 different concentrations) and water/ethanol. The second part of the work is related with traditional thermogravitational columns and numerical analysis of previously published experimental results. Again, mixtures regarding this part are the same as in the first part of the paper.

2. Thermogravitational microcolumn experimental setup

Experimental studies were performed in a paralelepipedic thermogravitational microcolumn [32]. The present configuration was used in the past for mixtures with Soret positive coefficients, in both steady state [33, 34] and transient parts of separation [35]. However, this was the first experimental analysis in which negative Soret coefficients were measured directly and instantaneously with purely optical systems. A brief explanation of the microcolumn setup can be found in [32-34] but, for clarity, Fig. 1 outlines the setup with the corresponding axes. Notice that d (0.51 mm) depicts the gap between both heated plates in the direction of x , L (30 mm) represents the height of the

microcolumn in the direction of z , and b (3mm) is the depth of the column in the direction of y . Concentration differences were measured experimentally along height L and extracted numerically at the shaded planes, which were at $L/10$ distance from the column ends. T_1 represents the temperature of a cold wall, while T_2 is the temperature of a hot wall. Angle γ represents inclination angle of the microcolumn.

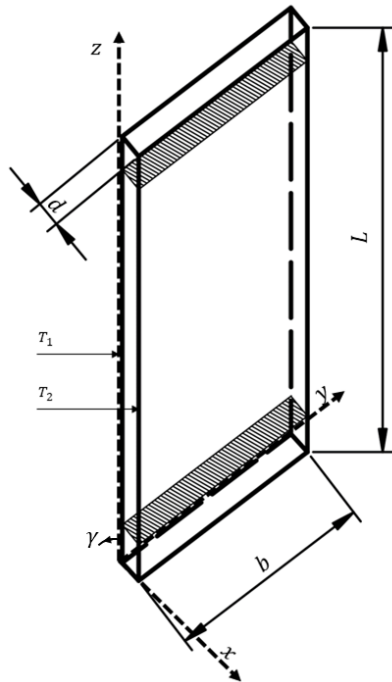


Figure 1. Outline of the microcolumn. Shaded planes are the planes of measure used here.

The analysed mixtures were toluene/methanol, water/ethanol in rich toluene and a water range where the Soret coefficient was negative. Fig. 2 shows composition details of these mixtures, and their thermophysical and transport properties are compiled in Table 1 [36, 37], where c_0 is the mean concentration of the denser component, ρ is the mean density of the mixture, β_c is the mass expansion, α is the thermal diffusivity.

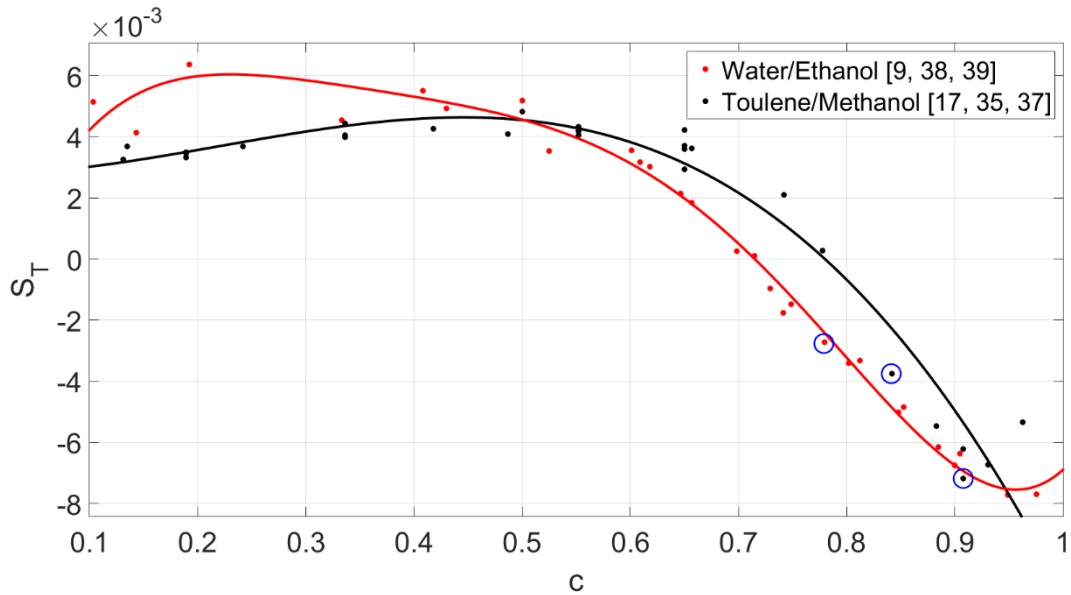


Figure 2. Soret coefficient in a toluene/methanol (black) [17, 35, 37] and water/ethanol (red) [9, 38] system through various concentrations. Mixtures analysed for this work are highlighted with blue circles. Lines are cubic polynomials fitted to the experimental data.

Table 1. Thermophysical properties of working mixtures at T=298.15K [16, 17, 36, 37]

Case/ Physical properties	Mixture 1	Mixture 2	Mixture 3
c_0 (toluene/toluene/water)	0.9080	0.8420	0.7796
$1-c_0$	0.0920	0.1580	0.2204
(methanol/methanol/ethanol)			
ρ (kg/m ³)	854.77	849.60	963.05
v (*10 ⁻⁷) (m ² /s)	6.38	6.62	19.20
β_T (*10 ⁻³) (K ⁻¹)	1.113	1.117	0.556
β_c (*10 ⁻²)	9.09	9.09	15.30
α (*10 ⁻⁸) (m ² /s ⁻¹)	9.56	9.56	11.73
D (*10 ⁻⁹ m ² /s)	1.14	0.90	0.79
D_T (*10 ⁻¹² m ² *K/s)	-8.20	-3.38	-2.14
S_T (*10 ⁻³ K ⁻¹)	-7.19	-3.75	-2.72

Table 2. Important ratios in the different mixtures used

Mixture	GrSc/A	S	tr/td	ΔT [K]	Gr
Toluene/Methanol (0.9080)	206	-0.0491	9	8	28.46

Toluene/Methanol (0.9080)	508	-0.0491	1.40	20	71.16
Toluene/Methanol (0.8420)	316	-0.0406	3.63	10	33.16
Toluene/Methanol (0.8420)	409	-0.0406	2.17	13	43.10
Toluene/Methanol (0.8420)	469	-0.0406	1.64	15	49.74
Toluene/Methanol (0.8420)	622	-0.0406	0.93	20	66.32
Water/Ethanol (0.7796)	38	-0.1287	257	6	1.17
Water/Ethanol (0.7796)	62	-0.1287	94	10	1.96
Water/Ethanol (0.7796)	95	-0.1287	43	15	2.94
Water/Ethanol (0.7796)	122	-0.1287	24	20	3.92
Water/Ethanol (0.7796)	152	-0.1287	16	25	4.90

Table 2 shows the values of parameter GrSc/A and separation S as well as the ratio between the relaxation time of the approach to the equilibrium and the relaxation time of the horizontal diffusion for the different mixtures analysed. The Grashof number is defined as $\text{Gr} = \frac{g\beta_T d^3 \Delta T}{v^2}$, the Schmidt number is defined as $\text{Sc} = \frac{v}{D}$ and A is the aspect ratio $\text{A} = \frac{L}{d}$. The relaxation time of the separation is defined as $t_r = \left(\frac{v}{\beta_T}\right)^2 \cdot \frac{9!L^2}{(\pi\Delta T g)^2 \cdot d^6} D$, while the relaxation time for horizontal diffusion is $t_d = \frac{d^2}{\pi^2 D}$. Separation parameter is defined as $S = \frac{D_T c_0 (1 - c_0) \beta_C}{\beta_T D}$. Those non-dimensional ratios, except separation parameter S are in function of temperature and for that reason they have different values for the same mixture. The literature has suggested that the critical numbers of the GrSc/A parameter for transient and steady state analyses are 200 and 1000, respectively [39]. Both critical values represent up to where transient and steady state approximations are correct. In addition, if the ratio t_r/t_d is greater than 10, the FJO theory is accomplished for the steady state. All the values from Table 2 are in the range of validity for steady state measurements, but not for transient measurements. It should be noted that the experiments with a GrSc/A higher than 200 overestimate the separation before reaching a steady state.

3. Numerical model

The numerical model used to simulate the paralelepipedic thermogravitational microcolumn and cylindrical traditional columns considers a Newtonian fluid under the Boussinesq approximation (constant thermophysical properties of the binary mixture except for the linear variation of density

with the temperature and concentration in the buoyancy term). In this way, the continuity, momentum and mass transfer balances are written as [34, 35]:

$$\nabla \cdot \mathbf{u} = 0 \quad (1)$$

$$\frac{\partial \mathbf{u}}{\partial t} + (\mathbf{u} \cdot \nabla) \mathbf{u} = -\frac{1}{\rho_0} \nabla p + \nu \nabla^2 \mathbf{u} + \vec{g} [1 + \beta_c (c - c_0) - \beta_T (T - T_0)] \quad (2)$$

$$\frac{\partial c}{\partial t} + (\mathbf{u} \cdot \nabla) c = D \nabla^2 c + D_T c_0 (1 - c_0) \nabla^2 T \quad (3)$$

$$\frac{\partial T}{\partial t} + (\mathbf{u} \cdot \nabla) T = \alpha \nabla^2 T \quad (4)$$

where ν represents kinematic viscosity, ρ_0 is mixture density, \mathbf{u} represents velocity vector $\mathbf{u} = (u, v, w)$, \mathbf{g} is vector of gravitational acceleration $\mathbf{g} = (0, 0, -g)$, $\mathbf{x} = (x, y, z)$ are vector coordinates and p is buoyant pressure (difference between total and hydrodynamic pressure). Initially c is set-up as mean c_0 concentration. No-slip impermeable boundary conditions for velocity \mathbf{u} are imposed at the six walls of the domain (see Fig. 1), zero gradient of concentration on four walls, with exception on two walls that are kept on constant temperature.

$$x = 0; \mathbf{u} = (0, 0, 0); T = T - \frac{\Delta T}{2}; \quad (5)$$

$$x = d; \mathbf{u} = (0, 0, 0); T = T + \frac{\Delta T}{2}; \quad (6)$$

On both walls, gradient of concentration is related with gradient of temperature.

$$D \frac{\partial c}{\partial x} + D_T \frac{\partial T}{\partial x} = 0 \quad (7)$$

To solve numerically the model, an OpenFOAM solver has been specifically constructed for this purpose [40]. The convective terms used a second order unbounded discretization while that the time integration was carried out based on a transient second order implicit Crank-Nicholson scheme with an off-centering coefficient equal to 0.9 to stabilize. The momentum and continuity equations have been solved using the PIMPLE algorithm and the temperature and concentration equations have been solved for each PIMPLE outer iteration securing the convergence. Neumann boundary conditions have been implemented with the help of the GroovyBC package [41]. Numerical solutions used in all cases the bi-conjugate gradient method preconditioned by incomplete Cholesky factorization or by the Diagonal-based Incomplete LU method. Initial conditions consider constant fields of velocity, temperature and concentration. The validity of the model have been extensively verified with numeric and experimental results in both Cartesian and cylindrical cases respectively [34,35,42]. Similar solver and numerical schemes have been used in our previous work regarding g-jitters influence on ternary mixture [43, 44].

4. Stability in paralelepipedic microcolumn

The results in the paralelepipedic microcolumn are presented separately for each mixture. In the first subsection, the most negative reported Soret coefficient for a mass fraction of toluene, $c_0 = 0.908$, is presented. These results focus on the flow characteristics, numerically showing that for higher temperature gradients, it is possible to stabilise the flow. Also, the numerical results are compared with two experimental results with temperature gradients of $\Delta T = 8\text{K}$ and $\Delta T = 20\text{K}$. In the second subsection, a more stable toluene/methanol mixture, i.e. Mixture 2, is examined. In this mixture, we confirmed experimentally the existence of a stability window for a certain time. By increasing the temperature gradient, the stability window widened. Finally, in the third subsection, results from the water/ethanol system are examined numerically and experimentally. For this mixture and under the conditions of the Cartesian coordinates, we were not able to reach a theoretical separation with any temperature gradient, neither experimentally nor numerically.

4.1. Mixture 1: Toluene/Methanol, $c_0 = 0.908$

The methanol mass fraction patterns, as a function of time and when a Soret negative coefficient is assumed, are presented in Fig. 3. One could see a similar separation phenomenon during the first seconds of the process when compared to the case of a positive Soret. The less dense component migrates to the cold wall and therefore concentrates on the bottom part of the column, while the denser component concentrates in the top part (see Figs. 3a and 3b). This ‘stationary’ separation remains roughly stable during a short period of time (stable time window) due to natural convection, which favours the stability of the adverse density gradient originated via the thermogravitational effect. However, for longer periods of time, the flow is destabilised, probably due to new convective currents in the horizontal direction combined with the influence of gravity on the denser component (see Figs. 3c and 3d).

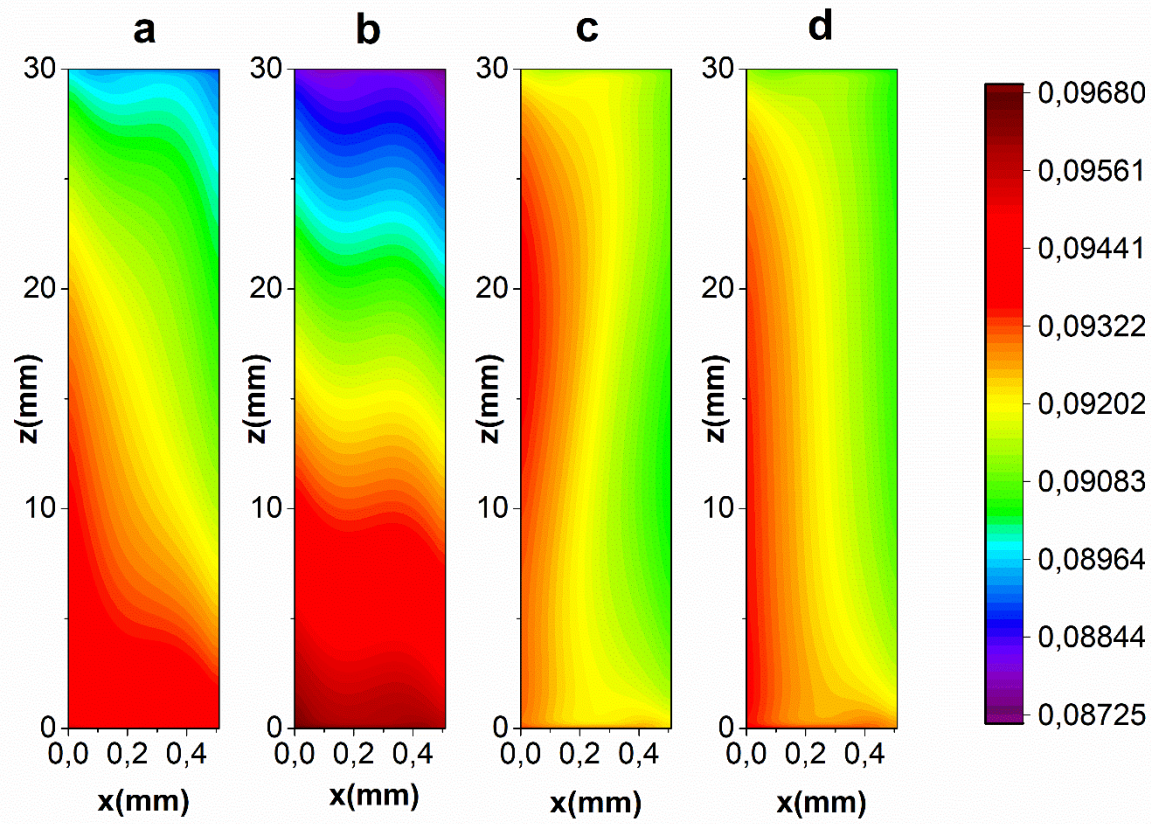


Figure 3. Methanol (Mixture 1) iso-concentration lines as a function of time, for the mid-XZ plane at $y=1.5\text{mm}$, $\Delta T=5^\circ\text{C}$ ($\text{Gr}=17.79$) and $b=3\text{mm}$: (a) $t=200\text{s}$, (b) $t=1200\text{s}$, (c) $t=1800\text{s}$ and (d) $t=2200\text{s}$.

As support of the information shown in the previous figure, Fig. 4 presents the concentration profiles in both the transient and stable time windows. Even though there are small fluctuations, during the stable window, the concentration profiles present a linear behaviour characteristic of the steady state (see Fig. 4, $t=1200\text{s}$), with a slight difference between slope values in the numerical solution ($m=0.3039$) and separation predicted by FJO theory ($m=0.2978$).

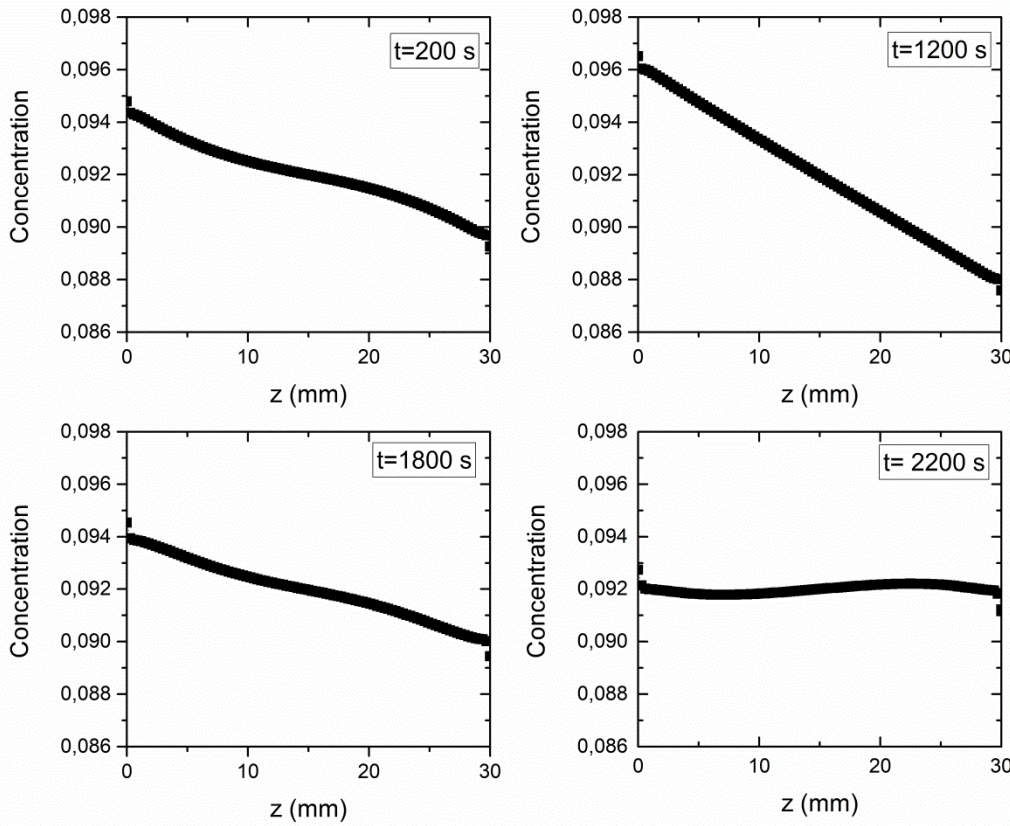


Figure 4. Vertical concentration profiles of methanol (Mixture 1) at $x=0.255\text{mm}$ and $y=1.5\text{mm}$.

Bou-Ali et al. [16] experimentally demonstrated that, for conventional cylindrical TG columns, an increase in the convection generates an increase in the duration of the stable window. This finding was also confirmed numerically using a TG microcolumn with paralelepipedic geometry (see Fig. 5). The numerical results in Fig. 5 involved Mixture 1 and data from Table 1. For $\Delta T=5\text{K}$, the stability window does not exist and hence actual separation barely reaches theoretical separation. For higher ΔT values, this window increases up to 1000s with $\Delta T=20\text{K}$. The size of the window remains similar for both 10K and 15K cases. In this regard, during the stability windows, the separation curve is rather stable, though small fluctuations appear. The separation Δc values of both $\Delta T=10\text{K}$ and $\Delta T=15\text{K}$ windows surpassed theoretical separation by a maximum of 2.7%. This error in Δc will translate to the same order of magnitude in the evaluation of the negative Soret coefficient.

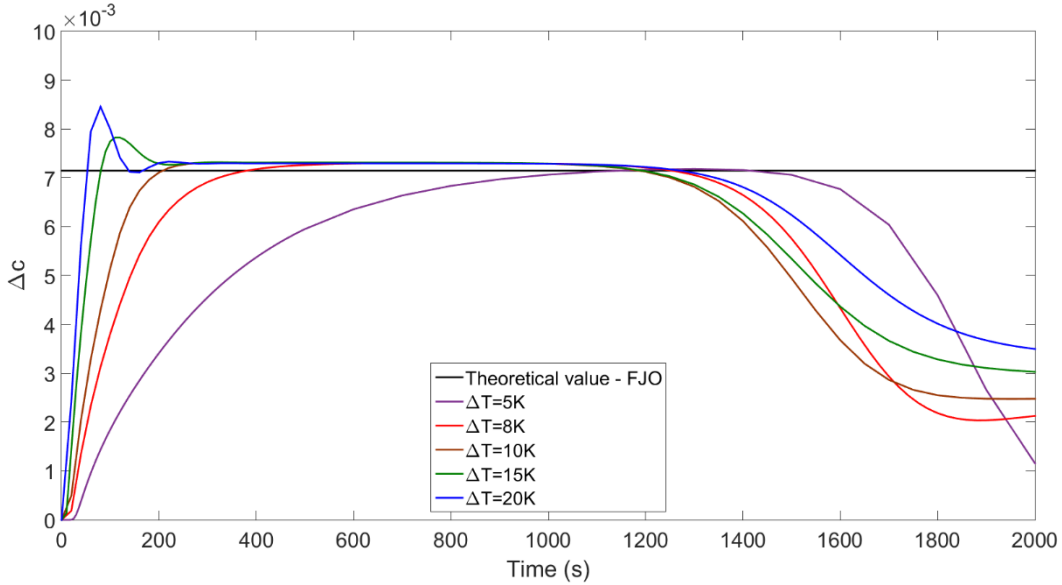


Figure 5. Separation stability windows for different initial temperature gradients for the microcolumn.

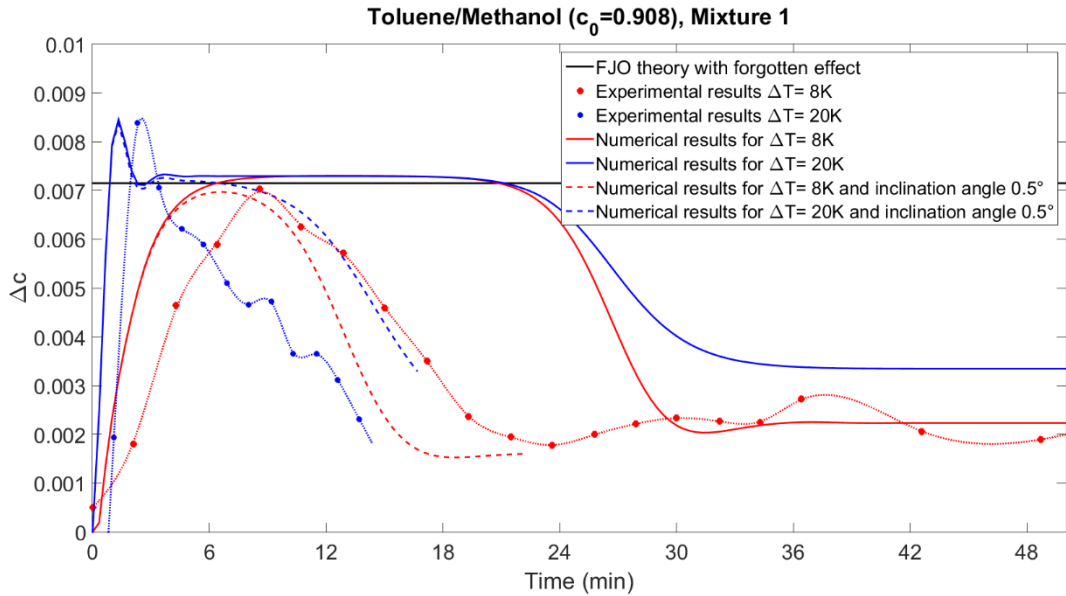


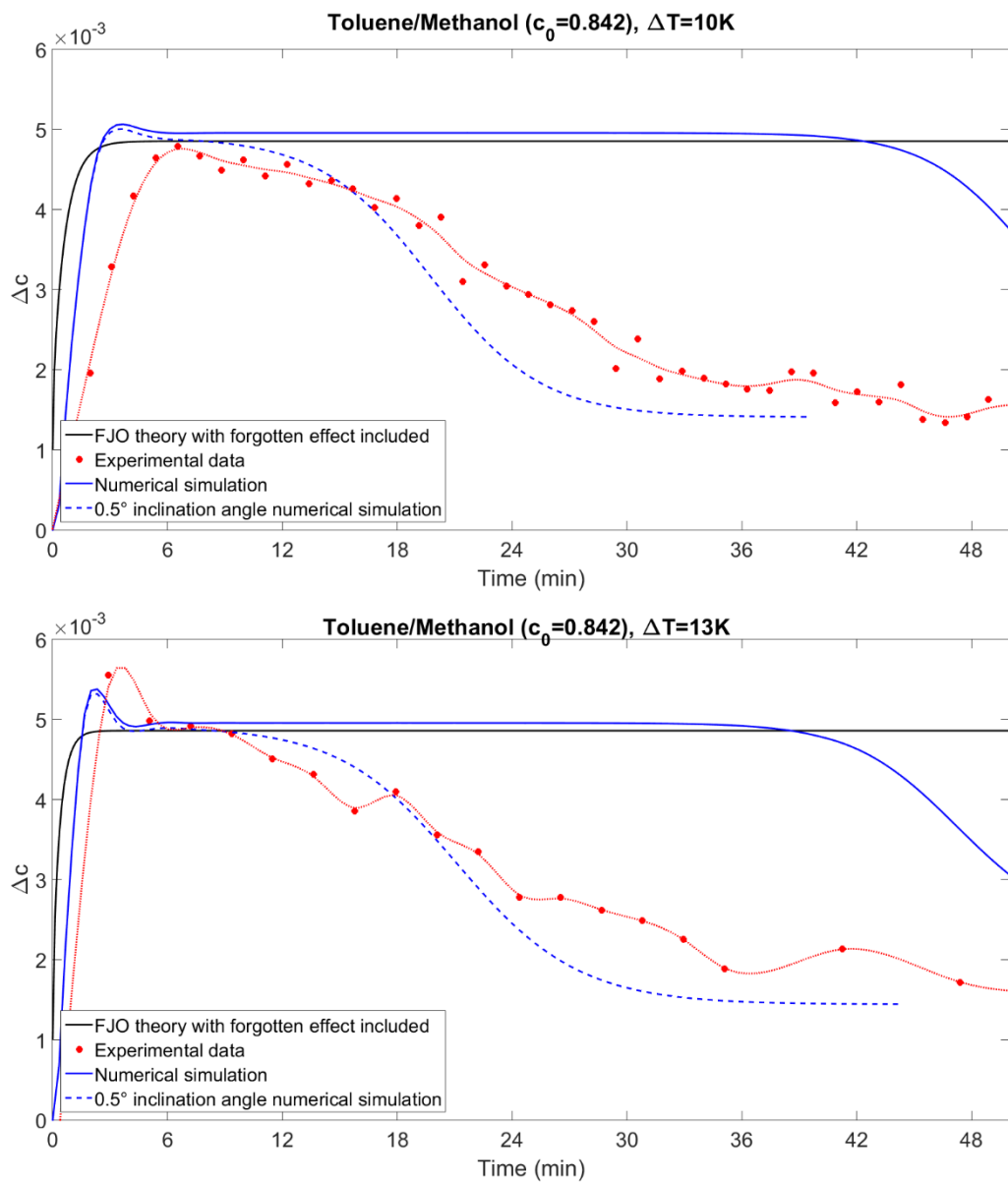
Figure 6. Experimental and numerical separation in Mixture 1 at 298.15K.

In order to check the numerical results, two experiments were carried out with Mixture 1 for $\Delta T=8\text{K}$ and $\Delta T=20\text{K}$ (see Fig. 6). From this figure, it is clear that the theoretical windows of stability were not experimentally obtained. As Mixture 1 is an extreme case in the value of the negative Soret coefficient, even a small imperfection in the experimental setup (see numerical results with an inclination angle of only $\gamma = 0.5^\circ$) could cause appreciable changes in the experimental separation curve. The orientation of γ is defined in Fig. 1. However, note the similar separation behaviour with both temperature gradients in the first part of the transient analysis. Case $\Delta T=8\text{K}$ reached a

steady state separation value, but was unable to maintain that separation for some time; meanwhile, case $\Delta T=20K$ presented an overestimation in both the experimental and numerical cases before a stable separation was reached, but only in the numerical case. Separation Δc is defined as difference between concentration values of integrated planes near top and bottom edge of the column.

4.2. Mixture 2: Toluene/Methanol, $c_0 = 0.842$

Since stability windows could not be observed experimentally using Mixture 1, another toluene/methanol mixture with a lower magnitude of the negative Soret coefficient was chosen. The thermophysical properties of Mixture 2 can also be found in Table 1. Four experimental runs were made using this mixture, with $\Delta T=10K$, $\Delta T=13K$, $\Delta T=15K$ and $\Delta T=20K$. In all runs, a stable time window was observed, except with $\Delta T=10K$. In this case, the separation did not reach the theoretical value (see Fig. 7).



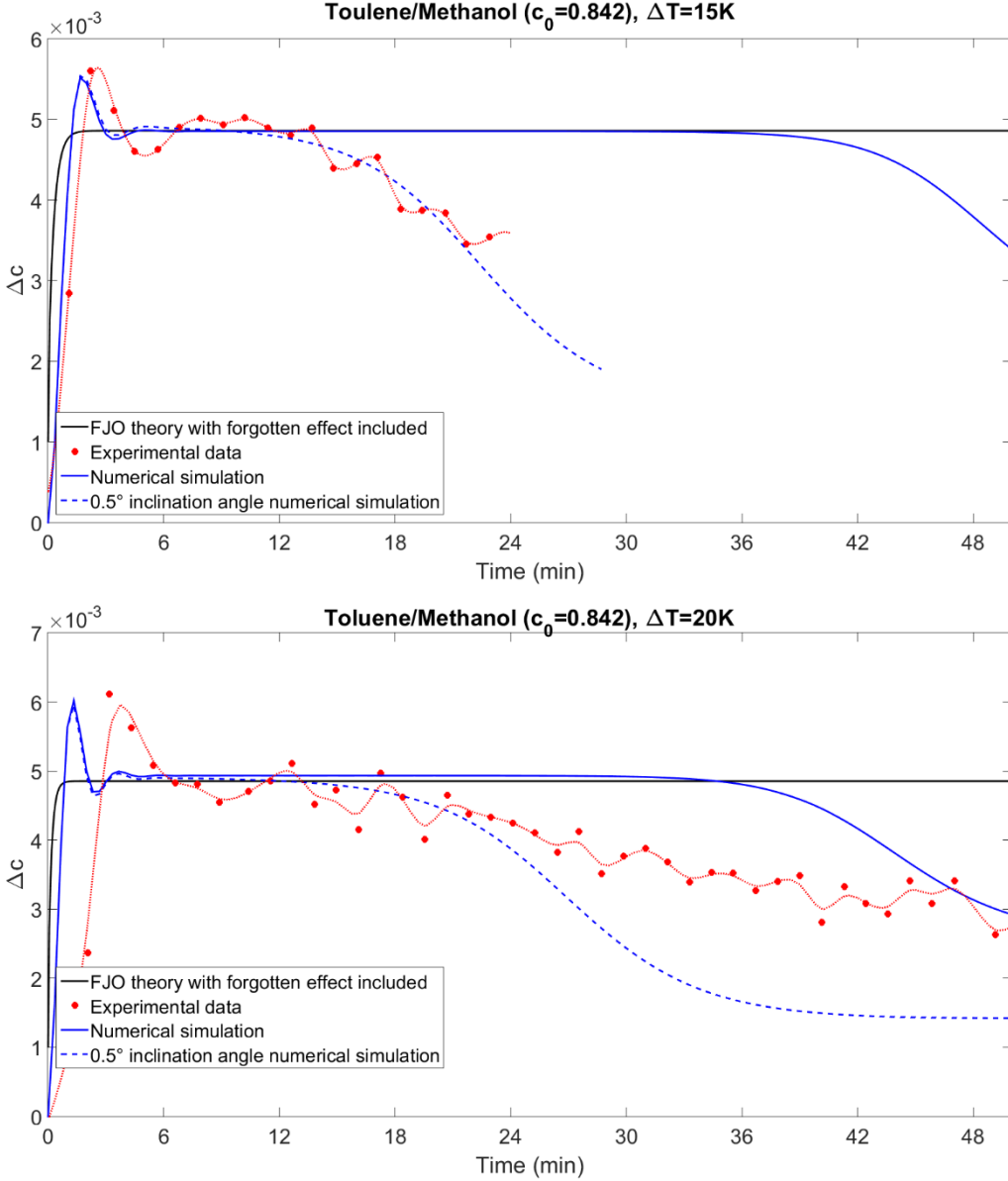


Figure 7. Stability of steady state separation for four different temperature gradients in Mixture 2 at $T_{\text{mean}}=298.15\text{K}$.

Figure 7 also shows that the longest window of stability was achieved, as expected, with the highest temperature gradient. With $\Delta T=20\text{K}$, the duration was approximately 15 minutes. With $\Delta T=15\text{K}$, the window was four minutes shorter. In the experiment with $\Delta T=13\text{K}$ ($\text{Gr}=43.11$), stability was achieved for roughly five minutes only. Comparatively, in Mixture 1 (see Fig. 5), numerically stable time windows were longer with a higher temperature gradient, which was not the case in Mixture 2 for the working temperatures considered. The duration of the stable time windows were of a similar magnitude. It seems that now, after a large enough temperature gradient ($\Delta T=10\text{K}$), there is no further improvement in the duration of the stability windows by increasing the gradient. The numerical window of stability was approximately twice as long as the experimental window for cases $\Delta T=15\text{K}$ and $\Delta T=20\text{K}$. The reasons for this discrepancy could be attributed to idealised conditions within the simulation, such as a zero inclination angle, perfectly flat surfaces, and a

constant and selected temperature gradient. In order to highlight the influence of the inclination angle on the stability of separation, numerical simulations were also run using an inclination angle of 0.5° in the y direction. As can be seen, these numerical solutions correlate well with the experimental results, explaining the apparent discrepancy between the experimental and numerical results without the inclination angle. Such a small inclination angle would not strongly affect experiments with positive Soret coefficients, as the density stratification is stable [34]. These results highlight how difficult it is to perform experiments with negative Soret coefficients under the thermogravitational effect.

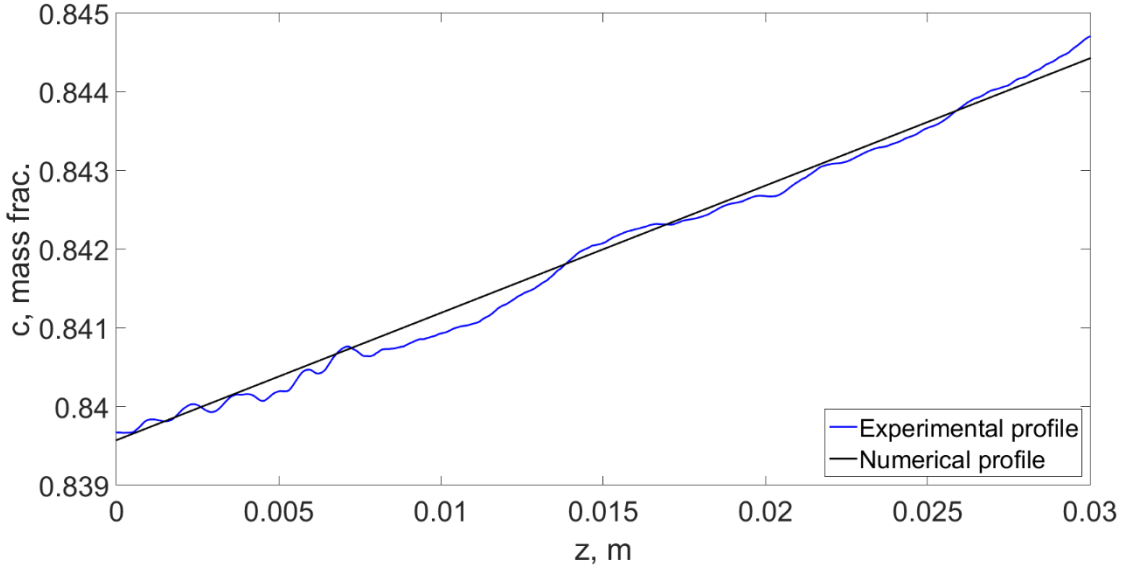


Figure 8. Comparison of experimental and numerical profiles along height in the window of stability at $t=10$ min for Mixture 2 and $\Delta T = 15K$ for Toluene component

Figure 8 demonstrates that during the window of stability, there is a certain level of linearity in the concentration profile, as is predicted by the FJO theory. The numerical results confirm that the concentration profile is fully linear, as predicted by FJO theory, along the height column during the stability window, without considering any inclination. However, in order to avoid confusion, it is necessary to highlight that this profile remains linear with separation of similar magnitude for twelve minutes.

Figure 9 presents the experimental concentration field with stable adverse stratification of the heavier component, toluene, which, in binary mixtures, means a stable adverse density stratification. Determination of the concentration profile was obtained using optical digital interferometry [33].

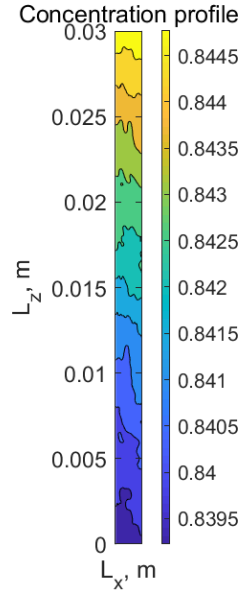


Figure 9. Experimental concentration field of toluene as a heavier component during the window of stability at $t=10$ min for Mixture 2 and $\Delta T = 15K$ ($Gr = 49.75$).

4.3. Flow stabilisation in toluene/methanol Mixtures 1 and 2

After conducting numerical simulations together with the experimental analysis, we investigated many different parameters that could lead to the stability of the flow and to a stable adverse stratification in the microcolumn. Higher temperature gradients gave us only the possibility of slightly increasing the window of stability in a reasonable range of temperature differences. However, in both simulations and experiments, after certain values of temperature gradients, the change is no longer significant. By an analysis of the numerical results, we concluded that instability arises due to the flow in the third direction, in which, according to FJO theory, the flow does not exist [45]. Velocity component y was examined in the upper cross-section ($z=0.027\text{m}$) through time for different cases, for both mixtures and temperature gradients. Mean velocity component was calculated for given cross-section. In all of them, once a significant increase in the velocity component y is observed, separation stability is diminished. This is plotted in Fig. 10 for $\Delta T = 10K$, with and without an inclination angle, in the case of Mixture 2. If the y component of velocity enhances unstable conditions in the column, then the inclination angle in the y direction could be the key parameter of the experimental destabilisation of separation occurring earlier than predicted in numerical simulations. In Fig. 10, it is also possible to see that a very small inclination angle strongly increases the y component of velocity, leading to unstable separation in the column.

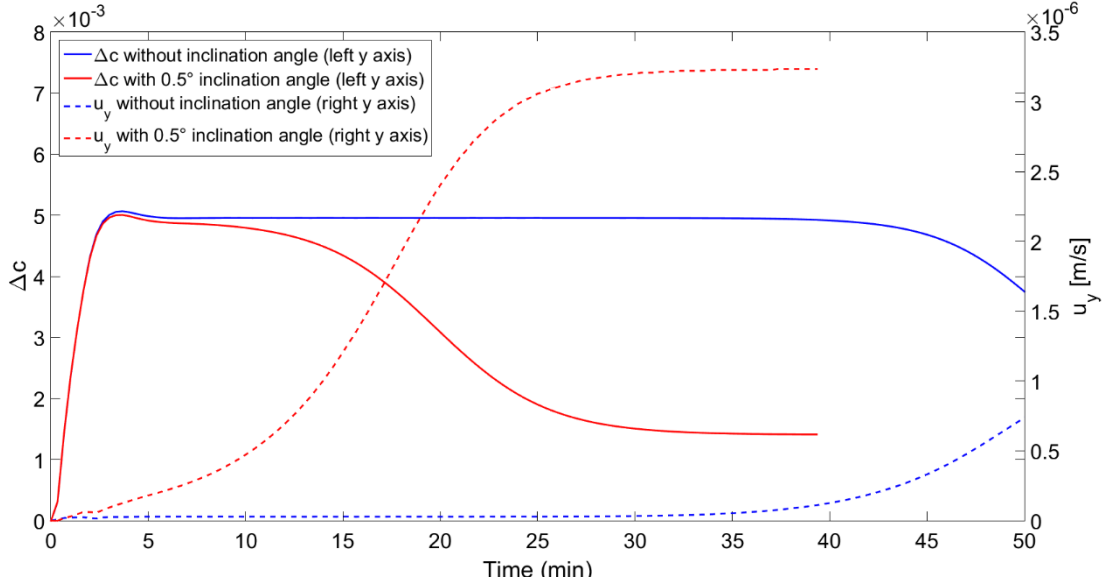


Figure 10. Concentration difference and velocity u_y in the upper cross-section for $\Delta T = 10K$ with and without an inclination angle (Mixture 2).

The coincidence of the time when separation decreases and the component of velocity u_y increases confirms results from Batiste et al. [22, Fig. 8e therein] where, in a cylindrical column, the maximum eigenvalue from linear stability analysis had the same growth rate as the azimuthal component of velocity.

As an increase in instability was related with an increase in velocity in the y direction, we simulated different values of breadth b . In this way, the separation predicted by FJO theory should remain the same, as we did not change the height h or the gap d , and the velocity in the y direction should be diminished. The value b , related with the present microcolumn geometry, was fixed at $b=3\text{mm}$. Simulations, apart from real geometry, were conducted for $b=2\text{mm}$, $b=1\text{mm}$ and $b=0.51\text{mm}$. The latter value means that the microcolumn has a square cross-section.

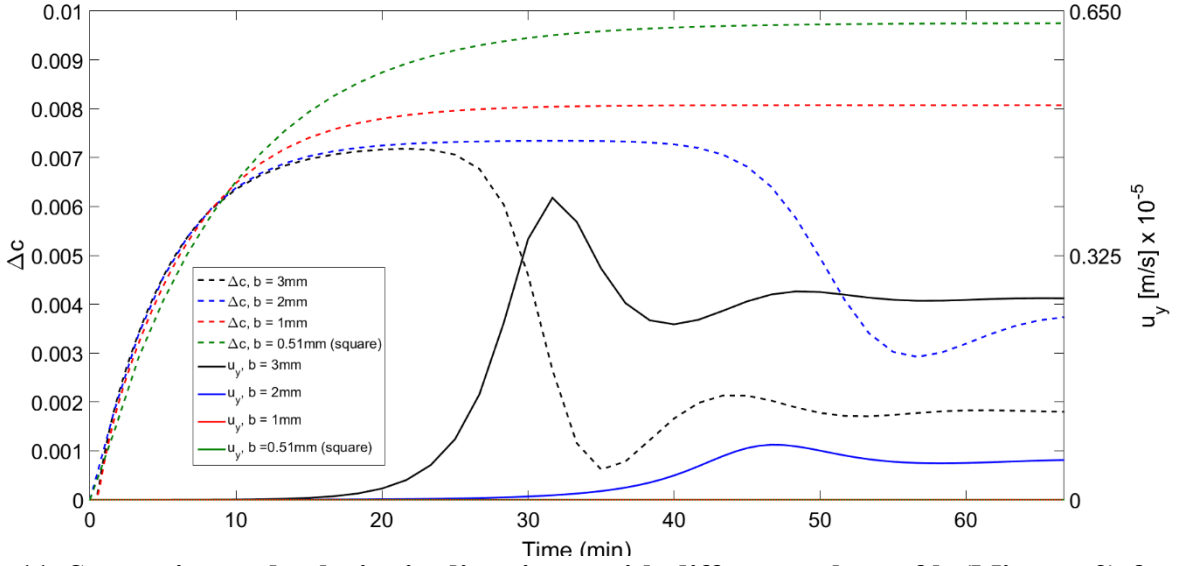


Figure 11. Separation and velocity in direction y with different values of b (Mixture 2) for $\Delta T = 10K$.

As can be seen from Fig. 11, stable separation was reached for $b=1\text{mm}$ and $b=0.51\text{mm}$. For the $b=2\text{mm}$, stability is longer than in the case of 3 mm, but it destabilised after approximately 2600s. In Fig. 11, we can see that for cases $b=0.51\text{mm}$ and $b=1\text{mm}$, u_y remained nearly 0. As these values are very close to 0 they can be appreciated from the Fig. 11. For the other two cases, the velocity u_y increment corresponded with perturbation in the concentration field steady state, with a small delay. Again, the conclusion is the same: an increase in velocity in the y direction is the cause of instability in the system.

In order to see if instability will grow in system where governing equations are not solved in the y direction, 2D cases are conducted. First, Mixture 1 $\Delta T = 10K$ case has been analysed since Mixture 1 is more unstable than Mixture 2. Also Mixture 1 is analysed in additional case, with $\Delta T = 5K$. In this case, separation parameter is adjusted to be 3/5 of the normal value, in order to check if there is any influence regarding this parameter. Comparison between results can be seen in Fig. 12.

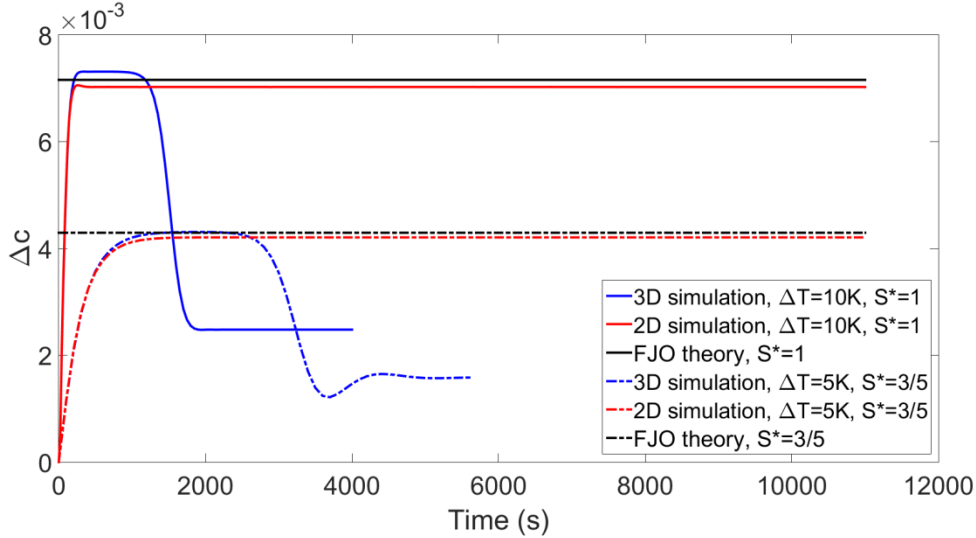


Figure 12: 2D simulation against 3D simulation

From Fig. 12, it can be seen that 2D simulation for very long time is stable (11000s) in both cases. In the contrary, instability in 3D simulation grows after approximately 1000s for the case $\Delta T = 10 K$ and about 2500s in the case $\Delta T = 5 K$. S^* is defined as relative separation parameter to Mixture 1 $S^* = S/S_{\text{mix}1}$. For the different values of S^* and $\Delta T = 5 K$, all 2D simulations were stable, as it can be seen on Fig. 13.

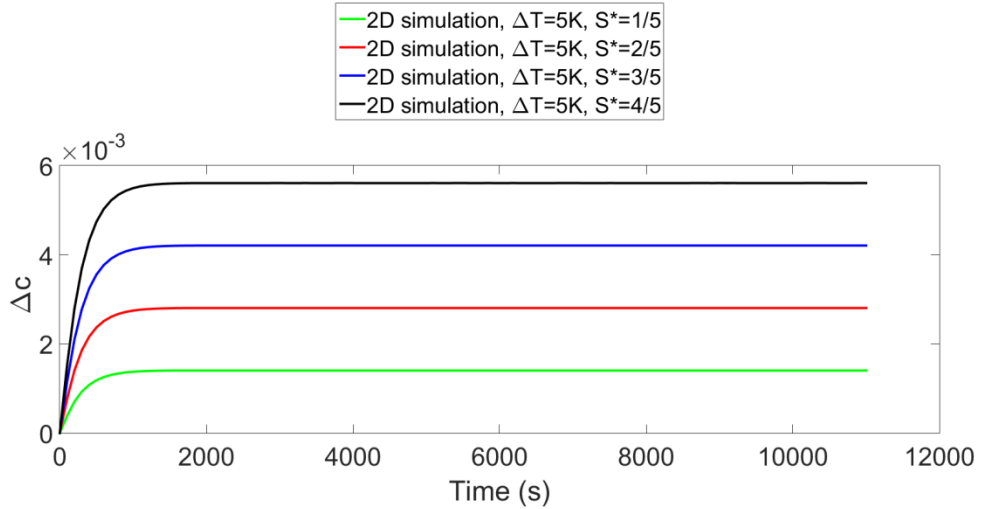


Figure 13: 2D simulation with different values of S^*

This justifies our assumption about reason behind instability in negative Soret experiments. Also, those results are again in accordance with [22], where system was stable against 2D perturbation and unstable against 3D perturbations.

A comparison between analytical solution for ideal mixture when forgotten effect is neglected provided in [28] and Mixture 1 with very small separation ratio can be seen in Fig. 14. Clearly,

there is difference between those two profiles. Numerical results for the profile are taken after “stability window” is broken, for the case $\Delta T = 8K$.

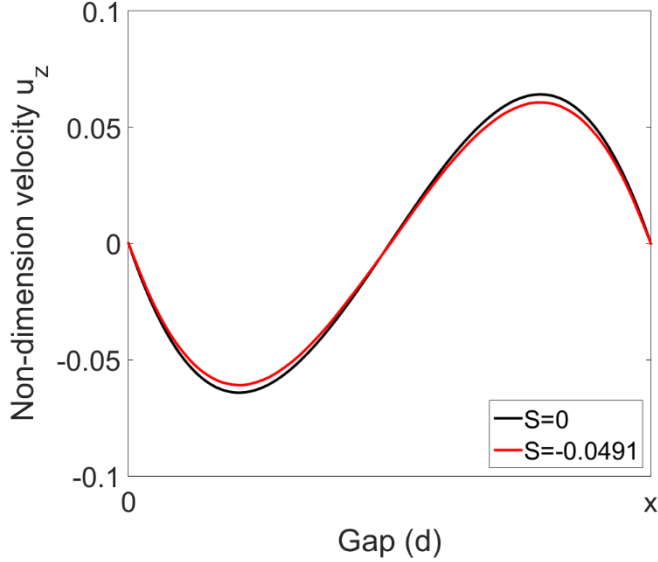


Figure 14: Comparison between velocity in z direction along the gap between ideal model with $S=0$ and numerical simulation of Mixture 1 for the $\Delta T = 8K$

4.4. Mixture 3: Water/Ethanol, $c_0 = 0.7796$

A water/ethanol mixture has significantly different thermophysical properties than toluene-methanol mixtures, especially viscosity, which is approximately three times higher. This means that the relaxation time for vertical separation t_r increases approximately nine times. In the experiments performed using this mixture, theoretical separation was not achieved for any temperature gradient in the microcolumn. The temperature gradients used in this case were $\Delta T = 6K$, $\Delta T = 10K$, $\Delta T = 15K$, $\Delta T = 20K$ and $\Delta T = 25K$. Regarding numerical results, presented simulations are for $\Delta T = 5K$, $\Delta T = 8K$, $\Delta T = 10K$, $\Delta T = 15K$ and $\Delta T = 20K$ on Fig. 15 compared with theoretical FJO approximation. Fig. 16 presents a comparison between numerical, theoretical and experimental separation. It is clear that in neither numerical simulations nor experiments did separation reach the theoretical value. This is in agreement with a previous explanation in this work, regarding toluene/methanol mixtures for slowly growing instabilities from the start of the experiment. As the relaxation time in this system is significantly higher, experiments in the microcolumn were unable to reach even theoretical separation because instability increased faster. This fact explains why certain mixtures for similar values of the parametric separation S show different behaviours. It was previously reported that parameter S is a key factor in establishing the window of stability, which, in our work, was not the case. On the other hand, numerical simulations agree with the experiments, although higher stability and separation were reached in the simulations, likely due to non-perfect conditions in the experimental setup. On the Fig. 16, forgotten effect refers to the situation that buoyancy force is also dependent on the compositional effects, and not only temperature field.

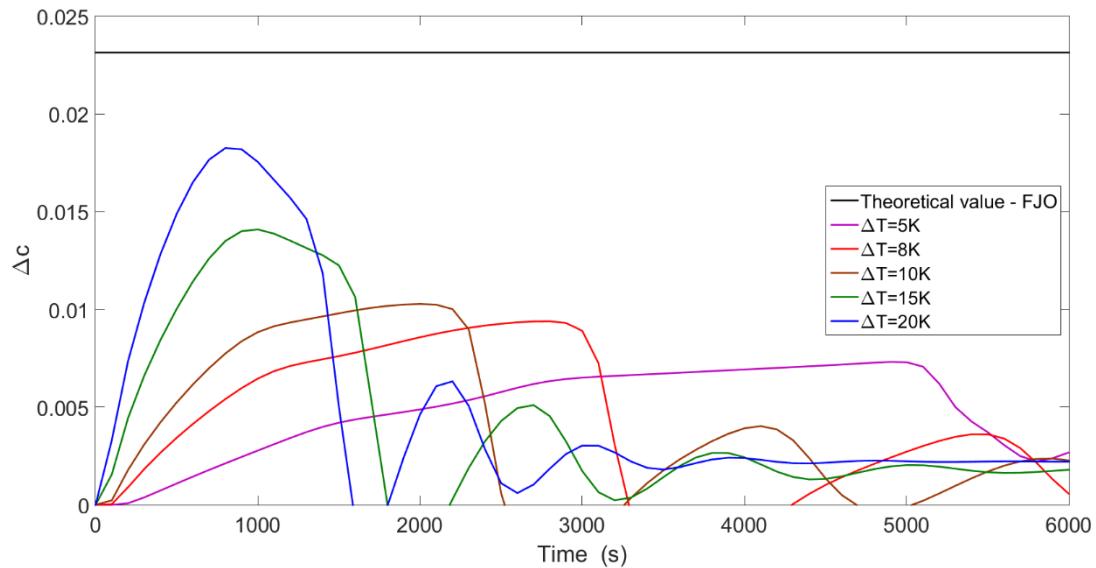


Figure 15. Comparison between numerical simulation and theoretical prediction for $\Delta T = 5 K$, $\Delta T = 8 K$, $\Delta T = 10 K$, $\Delta T = 15 K$ and $\Delta T = 20 K$ for Mixture 3

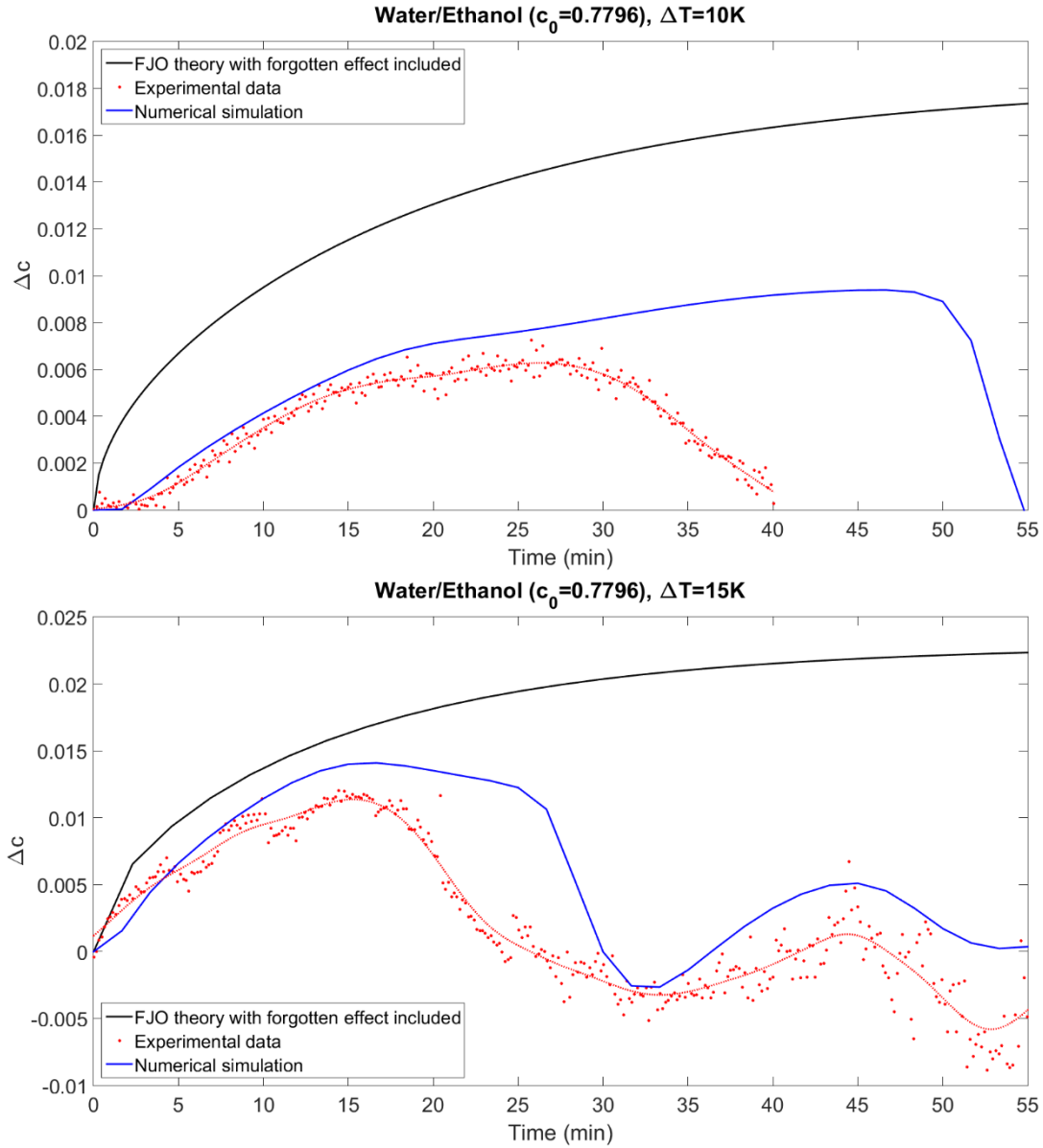


Figure 16. Comparison between numerical simulation, theoretical separation and experimental results with $\Delta T = 10K$ ($Gr = 1.96$) (up) and $\Delta T = 15K$ ($Gr = 2.94$) (down) for Mixture 3

In order to support statement that not only separation parameter S is related with stability in the system, few 3D simulations are conducted. Summary of those cases can be found in Table 3. Relative Grashof number Gr^* is defined as $Gr^* = Gr/Gr_{mix1}$, with Gr_{mix1} as Grashof number of mixture 1.

Case	S*	Gr*
1	1	1
2	2	1
3	1	2
4	1	3
5	3	1

Table 3: Summary of cases presented on Figure 17

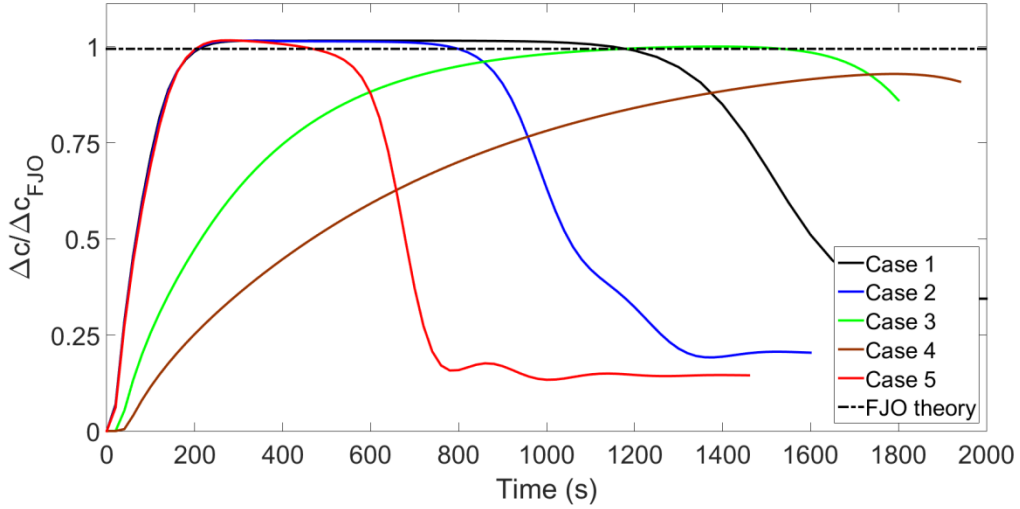


Figure 17: Plotted cases from Table 3 through time

As it can be seen from Fig. 17, although stability window was shorter with higher negative value of parameter separation, stronger influence was noticed in Case 3 and Case 4 compared to Case 1, where Grashof numbers were different. This is in accordance with our previous explanation inability where Mixture 3 was unable to reach steady-state was justified with higher viscosity of the system compared to Mixtures 1 and 2. Indeed, this could be the reason why stability window was longer with higher temperature gradient, as separation time is shorter.

In the Fig. 18, we have tried to summarize all the mixtures on one figure. In this figure Rayleigh solutal number is defined as in [16-17], $Ra_{sol} = \frac{\beta_T g L^3 \Delta c}{vD}$. Steady state vertical concentration gradient in uniform along microcolumn and can be define as $Ra_{sol} = 504SA^4$. It is important to highlight that comparing to [16] we operate on much lower Rayleigh solutal numbers as microcolumn has significantly smaller aspect ratio. Although we do not completely agree on their results [16], where $Gr_{crit} = 965|S|$ delineate stable from unstable region for the cylindrical configuration and not paralelepipedic, we agree on the importance of both parameters inside given formula. As we shown that any mixture is unstable against 3D perturbations, we will slightly change formulation and delineate region of where mixtures reach FJO predicted steady state value from those who never reach this value. In the manner of [16] it can be given as $Gr_{crit} = 181|S|$, where the last stable simulated mixture was taken as threshold. Red triangle markers on Fig. 18 represent mixtures that never reached stable separation, while blue x markers represent those that reached.

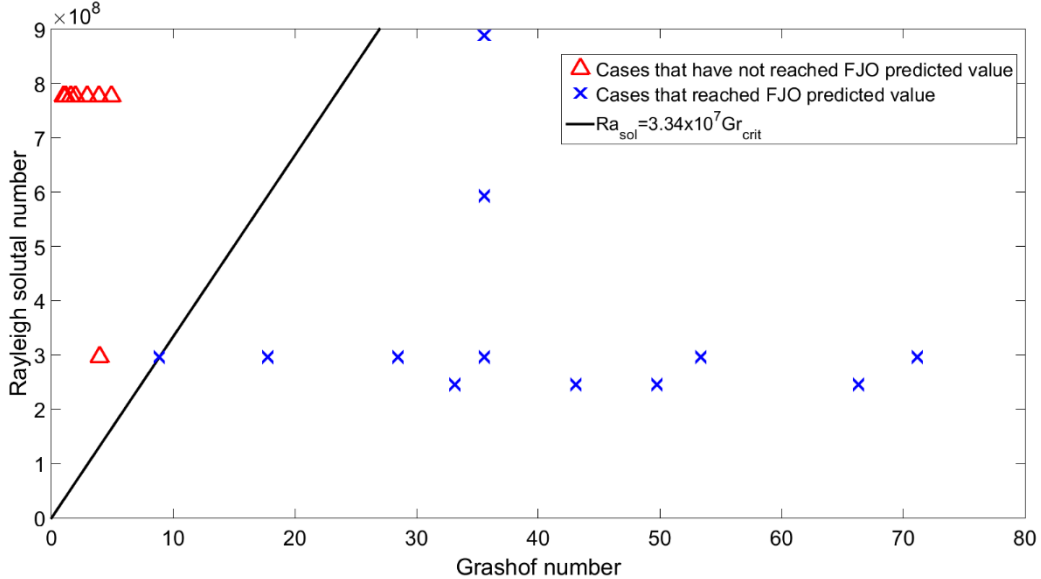


Figure 18: Mixtures that reached predicted FJO value (blue x markers) and mixtures that did not (red triangles)

5. Numerical analysis of separation stability in the cylindrical column

In this section, we present the numerical results of using the experimental initial conditions reported in [16] and compare them with the transient separation results obtained in that work. Many theoretical results [22, 24, 26] have indicated, through stability analysis, that instability will grow inside the column even for very high temperature gradients, which is contrary to what has been found experimentally [16, 17]. Full 3D numerical simulations were performed using the above-explained OpenFOAM solver for different initial conditions. To compare the numerical results as closely as possible to the experiments, we sought to mimic a fully experimental process. Experimentally, the extraction points were at $z = 6\text{cm}$ and $z = 48\text{cm}$. More information about experimental details can be found in [46]. In this work, extraction of the sample was of the order of 1 ml, with 0.5 ml as a minimum to determine the refractive index using a Pulfritch refractometer. In the numerical analysis, ‘extraction’ was of the order of 0.5 ml, with the same bottom points of extraction. The concentration in those volumes was averaged, and then the difference between the averaged values was compared to the experimental separation. An outline of the volumes and their relative positions inside the column can be found as shaded areas in Fig. 19. It is important to highlight that the numerical domain was 52cm, not 42cm, to avoid concentration nonlinearities near the column ends and, consequently, higher separation.

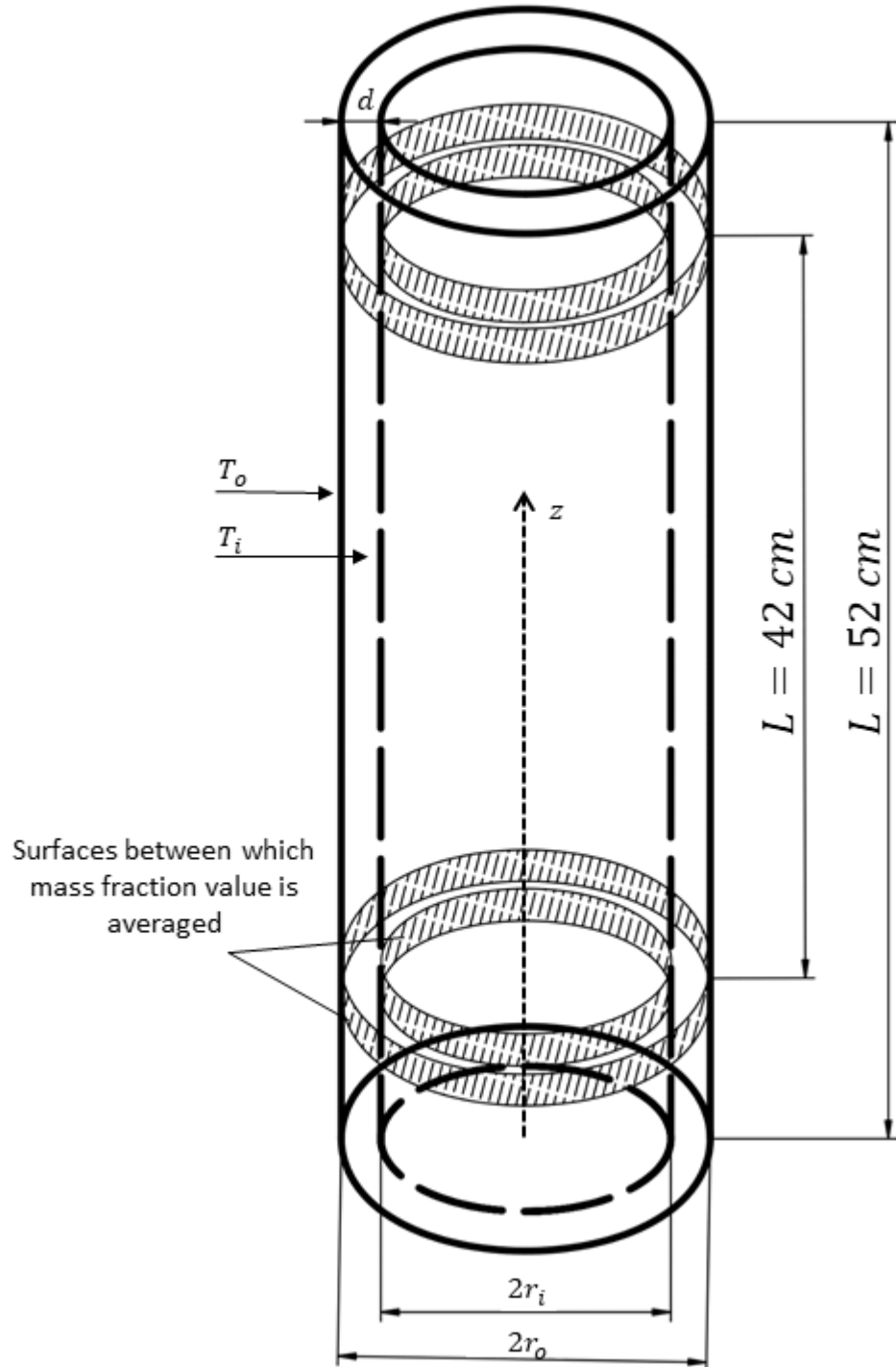


Figure 19. Outline of cylindrical thermogravitational column.

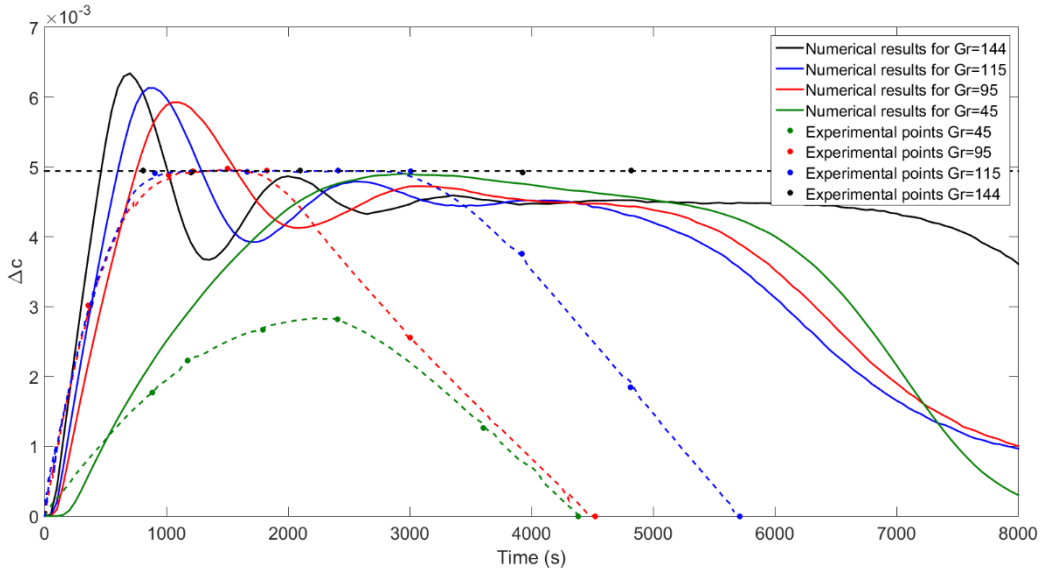


Figure 20. Numerical and experimental comparison for different Grashof numbers (different temperature gradients initially established on the walls).

The experimental results of Bou-Ali [16] concluded that in cylindrical thermogravitational columns, flow stability for Grashof numbers will be higher than critical, even for negative parametric separations. The experimental correlation [16] is

$$Gr_{crit} = 965|S|$$

where S is the parametric separation. In the case of the Mixture 3, the parametric separation is $S=-0.1297$, which leads to the conclusion that the critical Grashof number for this system is 124. However, the numerical results are in agreement with theoretical stability analysis showing that for numbers higher than the critical Grashof number, the flow inside the column is ultimately unstable. As evident from Fig. 20, for Grashof number 144, separation was stable for approximately 7000s, which is long enough to determine both steady state separation and thermodiffusion coefficients. Apparently, instability grows in the system immediately, but its development time is longer than the relaxation time of the system. This could potentially explain the apparent ‘steady state’, which was experimentally reported [16, 17]. Moreover, the transient thermogravitational technique is a very complex process prone to experimental errors. As the separation of species was tracked over time, for each value of separation, an independent experiment had to be run. For that reason, in Fig. 20, for each curve, we had 5–10 experimental points, which were not sufficient to fully explain the behaviour inside the column, especially for Grashof numbers below the critical value. The difference between the experimental and numerical steady state for $Gr=144$ was around 8%, which is an acceptable value. The reason for this discrepancy, apart from the slow growth of instability, could be the experimental determination of separation through measurement contrast factors, which in the case of cylindrical TG are refractive indexes. Later, the difference between refractive indexes was transformed into a concentration difference, which was later transformed into a concentration field. In order to compare the numerical results with the experimental results in this case, the temperature difference had to be accurately measured.

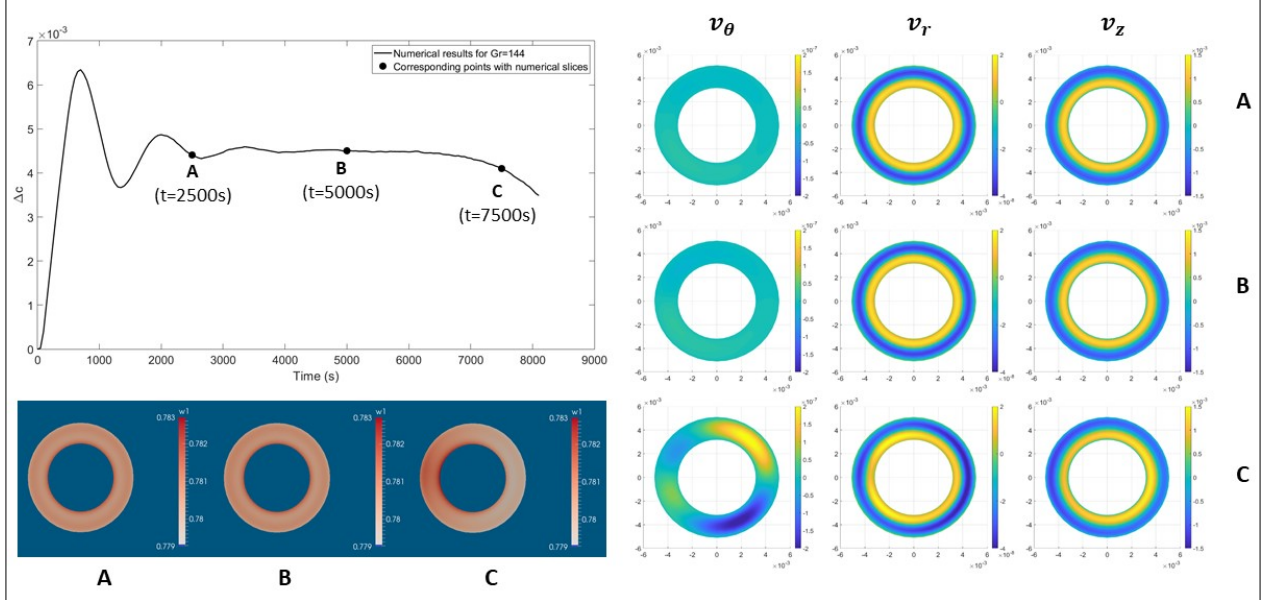


Figure 21. Numerical results at the $z = 6 \text{ cm}$ slice at the bottom extraction point for case of $\text{Gr}=144$

In Fig. 21, in the left upper part, the evolution of the concentration difference in case $\text{Gr}=144$ is represented. In the left bottom part, the concentration field at three different times is plotted in the bottom extraction slice. It is noticeable that for times A and B, where separation was still stable and instability had not grown enough to perturb the flow, the concentration field is axisymmetric. Water is more concentrated near the outer wall of the inner cylinder, which is the wall with a higher temperature. At point C, where instability had already changed the separation of water, the concentration field is not axisymmetric and is more concentrated on the left part of the space between tubes. On the right side, we represented azimuthal velocity, radial velocity and velocity in the z direction for three different times. The most interesting results are related with the azimuthal component of velocity, which is assumed to be 0 in FJO theory, ensuring that the flow is highly one-dimensional, except in the top and bottom of the column. However, for $t=7500\text{s}$, the azimuthal component grew and was approximately one order of magnitude higher than the values at $t=5000\text{s}$ and $t=2500\text{s}$. Due to this movement of liquid, the concentration field was perturbed and separation was destroyed.

Separation stability was examined for different mean diameters of the gap space between coaxial cylinders, as this value corresponds with the b value in the paralelepipedic geometry of the paralelepipedic microcolumn. By keeping the same gap and changing the ratio of curvatures, defined as $\delta = \frac{r_i}{r_o}$, where r_i is the inner radius and r_o is the outer radius, the mean diameter was changed. For the theoretical ratio $\delta \approx 1$, the mean diameter approaches to infinite, and the separation corresponded with the paralelepipedic geometry. On the other hand, when the ratio was $\delta \approx 0$, the mean diameter was approaches to 0, and separation was much different than theoretically predicted. The stabilisation of the flow was achieved in the same manner as in paralelepipedic geometry, by making b (mean radius) smaller. Geometry of the column used in Fig. 20 and Fig. 21 means that $\delta = 0.6213$. Consequently, this approach led to much different separation than that

assumed in FJO theory. In Fig. 22, this is represented for case $\text{Gr} = 45$ with a temperature gradient of $\Delta T = 3.25\text{K}$.

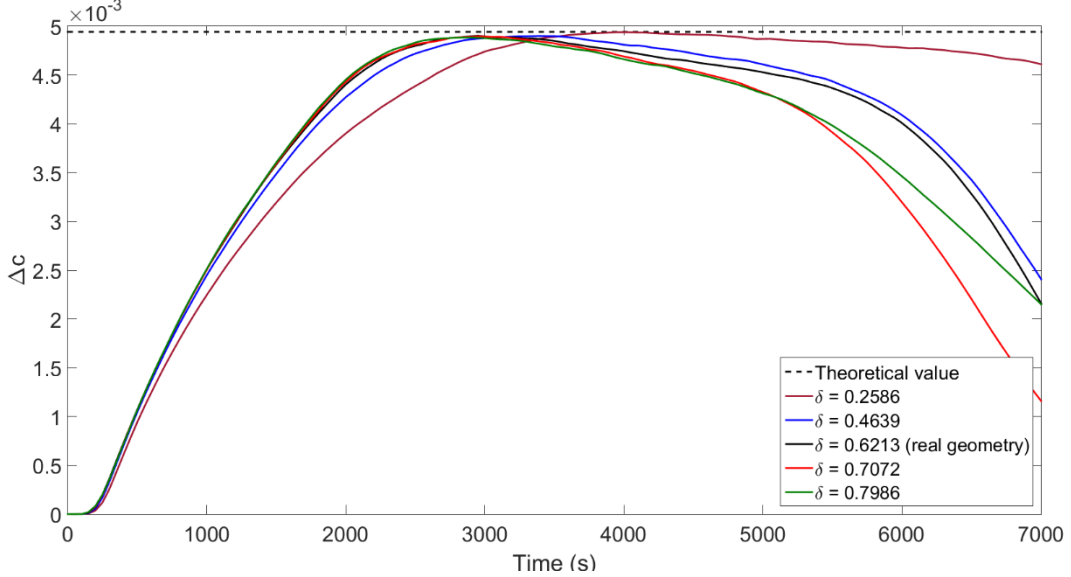


Figure 22. Separation in Mixture 3 with a constant gap and different values of the mean diameter and ratio of curvatures. Simulated cases consider $\text{Gr}=45$.

As can be seen from Fig. 22, separation tends to become stable for longer periods of time when the ratio of curvature is lower. On the other hand, for $t=2500\text{s}$, profiles of velocities in the z direction and the concentration field in the centre plane are represented in Fig. 23. We can see that, for values with a lower curvature ratio, separation is different than theoretically proposed. It is clear that due to the curvature, concentration differences are higher in the inner cylinder than in the outer one. The same pattern is observed for the velocity field, where the higher velocities are on the inner cylindrical side.

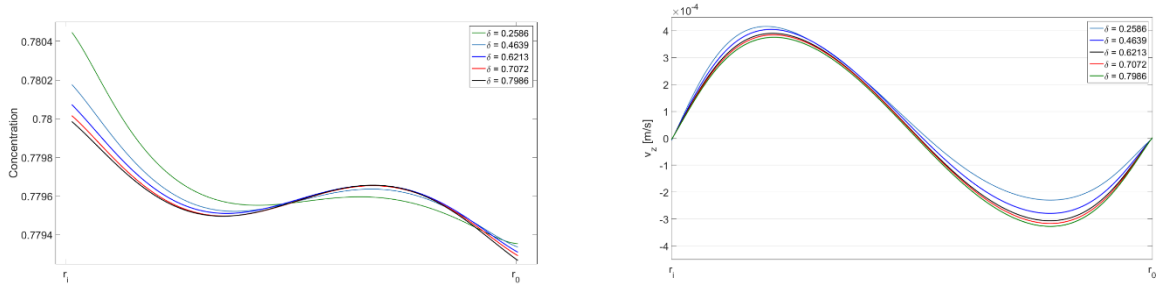


Figure 23. Concentration profile in the middle section for $z=0.26\text{m}$ (on the left) and velocity profile in the middle section for $z=0.26\text{m}$ (on the right). Simulated cases consider $\text{Gr}=45$.

In reference [17], negative thermodiffusion coefficients were obtained for different mixtures. Here, we examined Mixture 1 in the most extreme case. These experiments were conducted in another, slightly different cylindrical column, with a smaller gap between walls but a higher radius of cylinders. The Mixture 1 should be more stable than Mixture 3 since, for the same temperature gradients, it has a higher Grashof number due to a significant difference in the viscosity value.

Numerical results confirm this behaviour, where for $\Delta T = 10K$, stability was maintained up to $t=8000s$ (see Fig. 24) before the flow became unstable. Deviation from the theoretical separation was of the same order of magnitude as in the water/ethanol mixture.

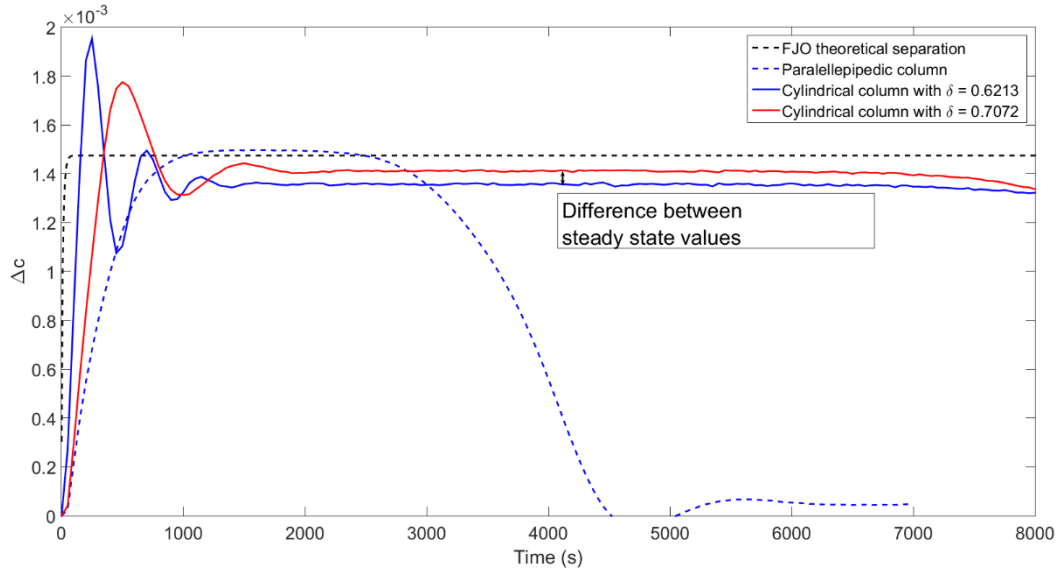


Figure 24. Separation for toluene/methanol Mixture 1 in two different types of cylindrical columns with the same height used in [14]. Cases are simulated with $\Delta T = 10 K$

A comparison between the stability in paralelepipedic and cylindrical columns with same heights and gaps is shown in Fig. 24. The paralelepipedic column tended to establish theoretical separation with a shorter stability window, while the cylindrical column, due to curvature, had slightly smaller separation but a longer stability window. This is a possible explanation for why experimental reports on negative Soret numbers are only related with cylindrical columns. On the other hand, the difference in separation during windows of stability could explain why, in [14], even for positive Soret numbers, there was a difference in the results obtained using columns with a different radius ratio. The effect of curvature on predominantly positive Soret numbers was explained in [26] with the same conclusion.

6. Conclusions

Separation stability was examined for different mixtures with negative Soret coefficient, in a paralelepipedic microcolumn, concluding that it was experimentally possible to achieve stable separation in Mixture 1 and Mixture 2 only for a short time. In the Mixture 3, it was not possible to obtain either a stable separation window or a theoretical value of separation due to the long relaxation time of the system. Numerically, for toluene/methanol mixtures, the stable separation time was a bit longer than that achieved experimentally. One possible explanation for this apparent discrepancy could be the non-perfect experimental conditions, which can disturb negative Soret experiments. Such non-perfect conditions include, for example, certain inclination angles of the column or a non-uniform temperature field. Simulations with an inclination angle of 0.5° in the y direction agreed well with the present experimental results. The importance of the neglected dimension in FJO theory (in our work denoted as b) was highlighted as a relevant stability factor.

It was shown that by changing the b dimension, stable separation can be achieved for a longer amount of time. This is done by minimising the velocity component in the direction of y, which is a crucial value needed for instability to grow inside the system. However, stable separation does not accord with FJO theory, and it is not suitable to obtain thermodiffusion coefficients in this case. The effect of a higher temperature gradient as a stabilisation factor was confirmed.

In the case of cylindrical columns, the experimental results obtained previously in the literature were compared with the numerical results. It was shown that the cylindrical column tends to maintain stable separation for a longer period of time; however, due to the effect of curvature, the values of stable separation were lower than the ones theoretically assumed. This is not the case only with negative Soret numbers, but also with positive values, as has been experimentally observed in previously published literature. The azimuthal velocity component was also found to be a crucial value in the case of the cylindrical column. When this component is almost zero, stable separation can be achieved for a much longer time. However, as in the previous case, by changing the mean diameter of the space between coaxial cylinders, separation is different than theoretically proposed. This value of the mean diameter is comparable to the b dimension in the paralelepipedic column. The behaviour of thermogravitational stability is similar for Cartesian and cylindrical conditions. However, as experimentally observed, the inclination effect influences the paralelepipedic configuration more than the cylindrical values. For further advancement, non-linear and linear stability analysis of the three-dimensional problems in cylindrical columns are necessary.

Acknowledgements

This work was supported by Ministerio de Ciencia, Innovación y Universidades and the European Regional Development Fund (FEDER) (grant numbers: ESP2017-83544-C3-1-P and ESP2017-83544-C3-3-P), DCMIX (AO-2009-0858/1056) from the European Space Agency, the Research Group Program (IT1009-16) from the Basque Government, FETRAFLU (2018-CIEN-000101-01) from the Gipuzkoa Program and the Universitat Rovira i Virgili (URV) grant number DLRF4741.

References

- [1] Soret, C. (1879). Archives des Sciences Physiques et Naturelles de Genève, t.II, p. 48-61.
- [2] Marcoux, M., Charrier-Mojtabi, M.C., Mojtabi, A., Costeseque, P. (2008). The influence of thermal diffusion on solar pond equilibrium.
- [3] Galliero, G., Bataller, H., Croccolo, F., Vermorel, R., Artola, P. A., Rousseau, B., Zhang, K. (2016). Impact of thermodiffusion on the initial vertical distribution of species in hydrocarbon reservoirs. *Microgravity Sci. Technol.*, 28(2), 79-86.
- [4] Gregg, M.C. (1973). The microstructure of the ocean, *Sci. Am.*, 228(2), 64-77.
- [5] Spiegel, E.A. (1972). Convection in stars II. Special effects, *Annu. Rev. Astron. Astr.* 10.1, 261-304.
- [6] Martin-Mayor, A., Bou-Ali, M. M., Aginagalde, M., Urteaga, P. (2018). Microfluidic separation processes using the thermodiffusion effect. *Int. J. Therm. Sci.*, 124, 279-287.

- [7] Platten, J.K. (2006). The Soret Effect: A review of recent experimental results. *J. Appl. Mech.*, 73.
- [8] Mialdun, A., Shevtsova, V. (2011). Digital interferometry as a powerful tool to study the thermodiffusion effect, *C.R. Mecanique*, 339, 362-368.
- [9] Koniger, A., Meier, B. Kohler, W. (2009). Measurement of the Soret, diffusion, and thermal diffusion coefficients of three binary organic benchmark mixtures and of ethanol-water mixtures using a beam deflection technique, *Phil. Mag.*, 89(10), 907-923.
- [10] Leppla, C., Wiegand, S. (2003). Investigation of the Soret effect in binary liquid mixtures by thermal-diffusion-forced Rayleigh scattering (contribution to the benchmark test), *Phil. Mag.*, 83(17), 1989-1999.
- [11] Platten, J.K., Marcoux, M., Mojtabi, A. (2007). The Rayleigh-Bernard problem in extremely confined geometries with and without the Soret effect. *C.R. Mechanique*, 335 638-654
- [12] Platten, J.K., Chavepeyer, G. (1973). Oscillatory motion in Bernard cell due to the Soret effects. *J. Fluid Mech.*, 60, 305-319.
- [13] Bou-Ali, M.M., Valencia, J.J., Madariaga, J.A., Santamaría, C., Ecenarro, O., Dutrieux, J.F. (2003). Determination of the thermodiffusion coefficient in three binary organic liquid mixtures by the thermogravitational method, *Phil. Mag.*, 83, 2011-2015.
- [14] Blanco, P., Bou-Ali, M.M., Platten, J.K., de Mezquia, D.A., Madariaga, J.A., Santamaría, C. (2010). Thermodiffusion coefficients of binary and ternary hydrocarbon Mixtures. *J. Chem. Phys.*, 132, 114506.
- [15] Caldwell, D.R. (1976). Thermosolutal convection in a solution with large negative Soret coefficient. *J. Fluid Mech.*, 74, 129-142.
- [16] Bou-Ali, M.M., Ecenarro, O., Madariaga, J.A., Santamaría, C.M., Valencia, J.J. (1999). Stability of convection in a vertical binary fluid later with and adverse density gradient. *Phys. Rev. E*, 59(1), 1250-1252.
- [17] Bou-Ali, M.M., Ecenarro, O., Madariaga, J.A., Santamaría, C.M., Valencia, J.J. (2000). Measurement of negative Soret coefficients in a vertical fluid layer with an adverse density gradient. *Phys. Rev. E*, 62(1), 1420-1423.
- [18] Rudakov, R.N. (1966). On small perturbations of convective motion between vertical parallel planes. *J. Appl. Math. Mech.*, 9, 362-368.
- [19] Rudakov, R.N. (1967). Spectrum of perturbations and stability of convective motion between vertical planes. *J. Appl. Math. Mech.*, 31, 349-355.
- [20] Nikolaev, B.I., Tubin, A.A. (1971). On the stability of convection motion of a binary mixture in a plane thermal diffusion column. *J. Appl. Math. Mech.*, 35, 248-245.
- [21] Gershuni, G.Z., Zhukhovitskii, E.M., Sorokin, L.E. (1983). On stability of convection flow of a binary Mixture with thermal diffusion. *J. Appl. Math. Mech.*, 46, 54-57.
- [22] Batiste, O., Alonso, A., Mercader, I. (2004). Hydrodynamic stability of binary mixtures in Bernard and thermogravitational cells. *J. Non-Equil. Thermody.*, 29, 359-375.
- [23] Zebib, A. (2007). Convective instabilities in thermogravitational columns. *J. Non-Equil. Thermody.*, 32, 211-219.
- [24] Zebib, A. (2008). Stability of ternary and binary mixtures in a vertical slot including the Soret effect. *J. Chem. Phys.*, 129, 134711.
- [25] Ryzkhov, I., Shevtsova, V. (2009). Long-wave instability of a multicomponent fluid layer with the Soret effect. *Phys. Fluids*, 21, 014102.
- [26] Ryzkhov, I., Shevtsova, V. (2009). Convective stability of multicomponent fluids in the thermogravitational column. *Phys. Rev. E*, 79, 026308.
- [27] Zebib, A., Bou-Ali, M.M. (2009). Inclined layer Soret instabilities. *Phys. Rev. E*, 79, 056305.

- [28] Haugen, K., Firoozabadi, A. (2005), On measurement of thermal diffusion coefficients in multicomponent mixtures, *J. Chem. Phys.* 122, 014516
- [29] Haugen, K., Firoozabadi, A. (2007), Transient separation of multicomponent liquid mixtures in thermogravitational columns, *J. Chem. Phys.* 127, 154507
- [30] Kozlova, S., Ryzhkov, I., (2016) On the separation of multicomponent mixtures in a cylindrical thermogravitational column, *Phys. Fluids* 28, 117102
- [31] Kozlova, S., Ryzhkov, I., (2018) The transient separation of multicomponent mixtures in a cylindrical thermogravitational column, *Int. J. Heat Mass Transf.* 126, 660-669
- [32] Naumann, P., Martin, A., Kriegs, H., Larrañaga, M., Bou-Ali, M.M., Wiegand, S. (2012). Development of a thermogravitational microcolumn with an interferometric contactless detection system. *J. Phys. Chem. B*, 116, 3889-13897.
- [33] Lapeira, E., Mialdun, A., Yanbu, V., Aretino, P., Shevtsova, V., Bou-Ali, M.M. (2018). Digital interferometry applied to thermogravitational technique, *Microgravity Sci. Technol.*, 30 635-641
- [34] Šeta, B., Lapeira, E., Dubert, D., Gavaldà, Jna., Bou-Ali, M.M., Ruiz, X. (2019). Separation under thermogravitational effects in binary Mixtures. *Eur. Phys. Rev. E*, 42(5).
- [35] Šeta, B., Gavaldà, Jna., Bou-Ali, M.M., Ruiz, X., Santamaria, C. (2020) Determining diffusion, thermodiffusion and Soret coefficients by the thermogravitational technique in binary Mixture with optical digital interferometry analysis, *Int. J. Heat Mass Tran.*, 147C, 118935
- [36] Lapeira, E., Bou-Ali, M.M., Madariaga, J.A., Santamaria, C. (2016). Thermodiffusion coefficients of water/ethanol mixtures for low water mass fractions. *Microgravity Sci. Technol.*, 28, 553-557.
- [37] Lapeira, E., Gebhardt, M., Triller, T., Mialdun, A., Kohler, W., Shevtsova, V., Bou-Ali, M.M. (2017). Transport properties of the binary mixture of the three organic liquids toluene, methanol and cyclohexane. *J. Chem. Phys.*, 146, 094507.
- [38] Kolodner, P., Williams, H., Moe, C. (1988). Optical measurements of the Soret coefficient of ethanol/water solutions. *J. Chem. Phys.*, 88, 6512.
- [39] Madariaga, J.A., Santamaria, C., Barutia, H., Bou-Ali, M.M., Ecenarro, O., Valencia, J.J. (2011). Validity limits of the FJO thermogravitational column theory: experimental and numerical analysis. *C.R. Mecanique*, 339, 292-296.
- [40] <https://openfoam.org/>
- [41] <https://openfoamwiki.net/index.php/Contrib/groovyBC>
- [42] Šeta, B., Errarte, A., Dubert, D., Gavalda, Jna., Bou-Ali, M.M., Ruiz, X., (2019), Gravitational stability analysis on double diffusion convection in ternary mixtures, *Acta Astronaut.*, 160 442-450
- [43] R. Jurado, J. Pallares, Jna. Gavalda, X. Ruiz, On the impact of the ISS reboosting maneuvers during thermodiffusion experiments of ternary liquid systems: Pure diffusion, *Int. J. Therm. Sci.* 132 (2018) 186-198
- [44] R. Jurado, J. Pallares, Jna. Gavalda, X. Ruiz, Effect of reboosting manoeuvres on the determination of the Soret coefficients of DCMIX ternary systems, *Int. J. Therm. Sci.* 142 (2019) 205-219
- [45] Furry, W.H., Jones, R.C., Onsager, L. (1939). On the theory of isotope separation by thermal diffusion. *Phys. Rev.*, 55, 1083.
- [46] Dutrieux, J.F., Platten, J.K., Chavepeyer, G., Bou-Ali, M.M. (2002). On the measurement of positive Soret coefficients. *J. Phys. Chem. B*, 106, 6104-6114.